Black Hole Excision for Dynamic Black Holes

Miguel Alcubierre[(1)], Bernd Brügmann[(1)], Denis Pollney[(1)], Edward Seidel[(1,2)], Ryoji Takahashi[(1)]
[(1)] *Max-Planck-Institut für Gravitationsphysik, Am Mühlenberg 1, D-14476 Golm, Germany*
[(2)] *National Center for Supercomputing Applications, Beckman Institute, 405 N. Mathews Ave., Urbana, IL 61801*
(February 7, 2008; AEI-2001-021)

We extend previous work on 3D black hole excision to the case of distorted black holes, with a variety of dynamic gauge conditions that respond naturally to the spacetime dynamics. We show that in evolutions of highly distorted, rotating black holes, the combination of excision and the gauge conditions we use is able to drive the coordinates to a frame in which the system looks almost static at late times. Further, we show for the first time that one can extract accurate waveforms from these simulations, with the full machinery of excision and dynamic gauge conditions. The evolutions can be carried out for long times, far exceeding the longevity and accuracy of better resolved 2D codes.

04.25.Dm, 04.30.Db, 97.60.Lf, 95.30.Sf

Introduction. The long term simulation of black hole (BH) systems is one of the most challenging and important problems in numerical relativity. For BHs, the difficulties of accuracy and stability in solving Einstein's equations numerically are exacerbated by the special problems posed by spacetimes containing singularities. At a singularity, geometric quantities become infinite and cannot be handled easily by a computer.

Traditionally, in the 3+1 approach the freedom in choosing the slicing has been used to slow down the approach of the time slices towards the singularity ("singularity avoidance"), while allowing them to proceed outside the BH [1]. Singularity avoiding slicings are able to provide accurate evolutions, allowing one to study BH collisions and extract waveforms [2], but only for limited evolution times. Combining short full numerical evolutions with perturbation methods, one can even study the plunge from the last stable orbit of two BHs [3]. But a breakthrough is required to push numerical simulations far enough to study orbiting BHs, requiring accurate evolutions exceeding time scales of $t \approx 100M$. In 3D, traditional approaches have not been able to reach such time scales, even in the case of Schwarzschild BHs. Characteristic evolution codes, on the other hand, are well-adapted to the long-term evolution of single black holes [4], but here we concentrate on non-characteristic methods for their ease of generalization to multiple black holes.

A more promising approach involves cutting away the singularity from the calculation ("singularity excision"), assuming it is hidden inside an apparent horizon (AH) [5,6]. This work has been progressing, from early spherical proof of principle [6] to recent 3D developments [4,7–10]. However, beyond a few spherical test cases [11,12], excision has yet to be used in conjunction with live gauge conditions designed to respond to both the dynamics of the BH and the coordinate motion through the spacetime.

In this paper we extend recent excision work [8] to the case of distorted, dynamic BHs in 3D, using a new class of gauge conditions. These gauge conditions not only respond naturally to the true spacetime dynamics, but also *drive the coordinates to a frame where the system looks almost static at late times.* We show that not only are the evolutions accurate as indicated by the mass associated with the apparent horizon, but also that very accurate waveforms can be extracted, even when the waves carry only a tiny fraction of the energy of the spacetime. We also show that the 3D evolutions of dynamic BHs we are now able to perform, are superior, in terms of accuracy, stability, and longevity, to previous 3+1 BH simulations, whether carried out in full 3D or even when restricted to 2D. These results indicate that BH excision can be made to work under rather general circumstances, and can significantly improve the length of the evolutions, and the accuracy of the waveforms extracted, which will be crucial for gravitational wave astronomy.

Initial Data. For this paper we consider single distorted BH spacetimes [13,14] that have been used to model the late stages of BH coalescence [15,16]. Following [13,14], the initial 3-metric γ_{ab} is chosen to be

$$ds^2 = \Psi^4 \left[e^{2q} \left(d\eta^2 + d\theta^2 \right) + \sin^2\theta \, d\phi^2 \right], \qquad (1)$$

where the "Brill wave" function q is a general function of the spatial coordinates, subject to certain regularity and fall off restrictions, that can be tailored to produce very distorted 3D BHs interacting with nonlinear waves. The radial coordinate η is logarithmic in the cartesian radius r. There are two classes of data sets used here corresponding to even- and odd-parity distortions. The even-parity data have vanishing extrinsic curvature, while the cases containing an odd-parity component have nontrivial extrinsic curvature K_{ij}. As shown in [17,18], these distorted BH data sets can include rotation as well, corresponding to spinning, distorted BHs that mimic the early merger of two orbiting BHs. Hence they make an ideal test case for the development of our techniques. We leave the details of the construction of these BH initial data sets to Refs. [17,18]. An important point that we wish to emphasize is that such data are *not* of the Kerr-Schild form with ingoing coordinates at the horizon. That form

of initial data sets has been recently advocated since it is not conformally flat [19] and is well adapted to inward propagation of quantities at the horizon.

Evolution and Excision Procedures. Our simulations have been performed using what we refer to as the "BSSN" version of the 3+1 evolution equations [20–23], which we have found to have superior stability properties when compared to standard formulations. As detailed in [22–24], we actively force the trace of the conformal-traceless extrinsic curvature $\tilde{A}_{ij}$ to remain zero, and we use the independently evolved "conformal connection functions" $\tilde{\Gamma}^i$ only in terms where derivatives of these functions appear. All the simulations described below have been performed using a 3-step iterative Crank-Nicholson scheme and a radiative (Sommerfeld) outer boundary condition. We refer the reader to Ref. [24] for the details of the numerical implementation.

We use the simple excision approach described in [8]. Our algorithm is based on the following ideas: (a) Excise a *cube* contained inside the AH that is well adapted to cartesian coordinates; (b) Use a simple boundary condition at the sides of the excised cube: copying of time derivatives from their values one grid point out along the normal directions; (c) Use centered (non-causal) differences in all terms except for advection terms on the shift (terms of the form $\beta^i \partial_i$). For these terms we use second order upwind along the shift direction. These simplifications in excision reduce the complexity in the algorithm, avoid delicate interpolation issues near the excision boundary, and have allowed us to make rapid progress. Currently, the method is implemented for non-moving excision regions, although they are allowed to grow. One can hope that colliding black holes can be treated even with this restriction through the use of co-moving coordinates. A more detailed description of our excision algorithm can be found in Ref. [8].

Gauge Conditions. For the lapse we use a hyperbolic slicing condition motivated by the Bona-Massó family of slicing conditions [25],

$$\partial_t \alpha = -\alpha^2 \, f\,(\alpha) \; (K - K_0), \tag{2}$$

where K is the trace of the extrinsic curvature, K_0 is its value in the initial data, and f is a (positive) function of α which we specify below. With this condition, the lapse will evolve as long as $\alpha^2 f(\alpha)$ and $K - K_0$ are non-vanishing.

For the shift β^i we have considered families of elliptic, parabolic, and hyperbolic conditions that relate the shift with the evolution of the conformal connection functions $\tilde{\Gamma}^i$. We obtain parabolic and hyperbolic shift conditions by making either $\partial_t \beta^i$ or $\partial_t^2 \beta^i$ proportional to the elliptic operator for β^i contained in the "Gamma freezing" condition $\partial_t \tilde{\Gamma}^k = 0$ (see Ref. [24]), itself closely related to the well known minimal distortion family [1]. Elliptic conditions have the disadvantage of requiring boundary data at the excision region where it is difficult to know what to impose, while parabolic conditions force a strong restriction on the stability of the differencing scheme: $\Delta t \propto (\Delta x)^2$ (this is true for explicit schemes, implicit schemes have no such restriction). We have then concentrated on hyperbolic conditions of the form

$$\partial_t^2 \beta^i = \zeta \, \partial_t \tilde{\Gamma}^i - \xi \, \partial_t \beta^i \,, \tag{3}$$

where ζ and ξ are positive functions. We call such evolution conditions for the shift hyperbolic "driver" conditions (see [26]).

In the spirit of the puncture method for evolutions [27], we use a BSSN scheme with the usual time-dependent conformal factor $e^{4\phi}$ and an additional time-independent conformal factor Ψ^4 that comes from the initial data. In our examples we use $\zeta = k/\Psi^4$, where k is a positive constant. The division by Ψ^4 helps to slow down the evolution of the shift in the vicinity of the black hole. We have found it important to add a dissipation term with a constant coefficient ξ in order to reduce some initial oscillations in the shift. Notice that in contrast with k, the coefficient ξ is not dimensionless (it has dimensions of inverse length), so in practice we rescale it using the total mass of the system. Experience has shown that by tuning the value of ξ we can almost freeze the evolution of the system at late times.

The parameters used for all simulations described below are: α is given by Eq. (2), with $f = 2/\alpha$; β^i is given by Eq. (3) with $\zeta = 0.75/\Psi^4, \xi = 3/M$ (M is the initial ADM mass of the system). As initial conditions we take $\alpha = 1$, $\beta^i = 0$, $\partial_t \alpha = \partial_t \beta^i = 0$, except in one case mentioned below where we perform a single maximal slicing solve to obtain a more appropriate initial lapse. Given these initial conditions, we let the gauge conditions take care of the rest. We use the same gauge parameters for all results in this paper, whether they are applied to Schwarzschild, distorted, or rotating BHs, showing the strength and generic nature of these conditions.

Results. The first example we show is Schwarzschild, written in the standard isotropic coordinates used in many BH evolutions. Note that with this initial data and our starting gauge conditions, the BH should evolve rapidly. If α and β^i were held fixed at their initial values, the slices would hit the singularity at $t = \pi M$. Instead, α and β^i work together with excision to rapidly drive the coordinates to a frame where the system looks essentially static, corresponding to the true physical situation.

In Fig. 1 we show the radial metric function g_{rr}/Ψ^4 vs. time. The grid covers an octant with 128^3 points ($\Delta x = 0.2$, $M = 2$). Appropriate symmetry conditions are applied on the faces of the octant for the different dynamical variables. We have checked that removing the octant symmetry (while using a lower resolution) does not change the results for the evolution times reported here (in particular no instabilities were encountered, cmp. [8]). Notice that the metric begins to grow, as it does without a shift, but as the shift builds up the growth slows down significantly. At this stage, the system is effectively static, even though we started in the

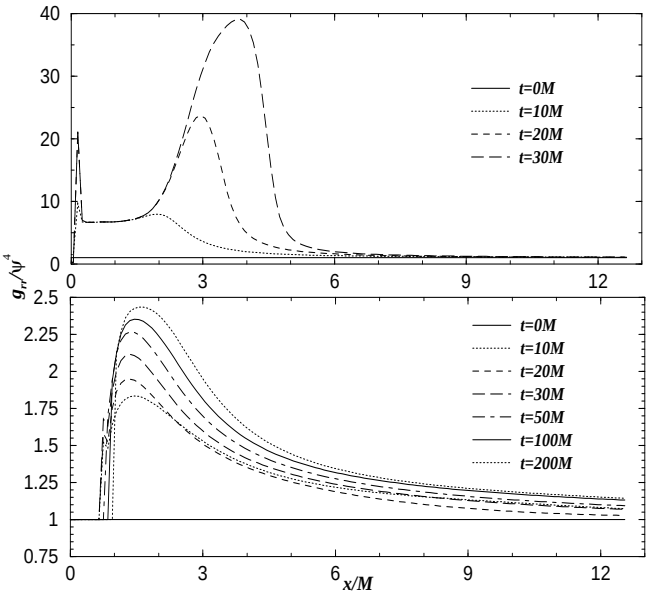

FIG. 1. We show the evolution of the radial metric function g_{rr}/Ψ^4 for a Schwarzschild BH along the $x-$axis, constructed from the cartesian components. The upper panel shows the grid stretching in the metric for singularity avoiding slicing with vanishing shift and no excision, while the lower panel shows the metric for the new gauge conditions with an excision box inside a sphere of radius $1M$. Note the difference in the vertical scales. Without shift and excision the metric grows out of control, while with shift and excision a peak begins to form initially but later freezes in as the shift drives the metric to a static configuration (note the time labels).

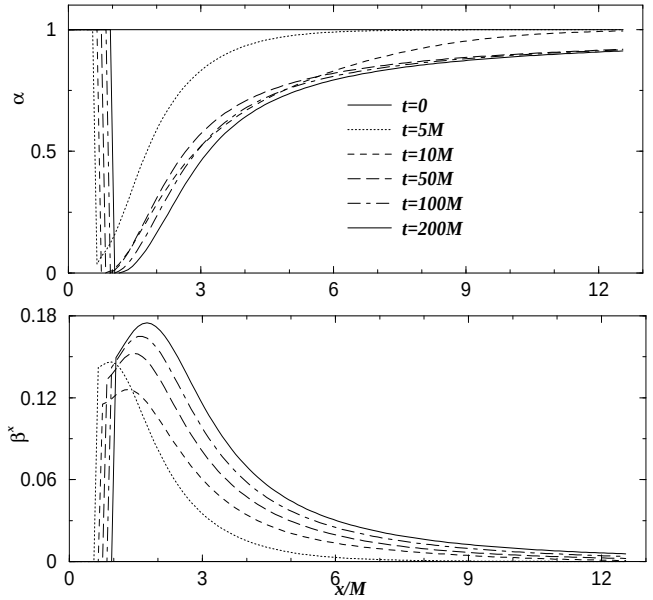

FIG. 2. We show the lapse and shift for the excision evolution of a Schwarzschild BH. After around 10M, the lapse and shift freeze in as the metric is driven to a static configuration. The size of the excision box was allowed to grow with the change in the coordinate location of the AH.

highly dynamic isotropic coordinates. We also show the time development of α and β^r in Fig. 2, which evolve rapidly at first but then effectively freeze, bringing the whole system to an almost static state by $t = 10M$. The evolution of the metric and gauge variables then proceeds only very slowly with time until the simulation is stopped well after $t = 200M$. The decision to stop the code at this time is simply a CPU time consideration, but we notice that in this and all following examples the code is stopped once all the interesting dynamics have finished.

Figure 3 shows the AH mass $M_{AH} = \sqrt{\text{Area}_{AH}/16\pi}$, determined with a 3D AH finder [28]. For comparison we also show the value of M_{AH} for the 3D run without shift, and for a highly resolved 2D simulation with no shift and no excision [14]. The 2D code uses maximal slicing, so the coordinate time t refers to different slices, but the slicings turn out to be even more similar than is to be expected from Eq. (2). While the 3D simulation with shift and excision continues well beyond $t = 200M$, the 2D result becomes inaccurate and the code crashes due to axis instabilities by $t = 150M$, and the 3D run without shift crashes already by $t = 50M$. Notice that in the 2D case, after around $t = 35M$, M_{AH} grows rapidly due to numerical errors associated with grid stretching. With excision and our new gauge conditions, the 3D run has less than a few percent error by $t = 200M$, while the 2D case has more than 100% error before it crashes at $t \approx 150M$. For the excision run, notice also that while there is some initial evolution in the metric and the coordinate size of the AH (see Figs. 1 and 2) the AH mass changes very little.

Next, we turn to a truly dynamic, even-parity distorted BH. This system contains a strong gravitational wave that distorts the BH, causing it to evolve, first nonlinearly, and then oscillating at its quasi-normal frequency, finally settling down to a static Schwarzschild BH. This provides a test case for our techniques with dynamic, evolving BH spacetimes, and allows us to test our ability to extract gravitational waves with excision for the first time. In this case, in the language of [17], we choose the Brill wave parameters to be $Q_0 = 0.5$, $\eta_0 = 0$, $\sigma = 1$, corresponding to a highly distorted BH with $M = 1.83$. Just as before, we use a grid that covers one octant, with 128^3 points and $\Delta x = 0.2$

In Fig. 4 we show the AH mass M_{AH} as a function of time for the distorted BH simulations carried out in both 2D and 3D. M_{AH} grows initially as a nonlinear burst of gravitational waves is absorbed by the BH, but then levels off as the BH goes into a ring-down phase towards Schwarzschild. Fig. 5 shows the proper polar circumference of the AH divided by its proper equatorial circumference. This ratio allows an estimate of the size of the local dynamics during the run. Notice how the horizon starts far from spherical (with a ratio close to 2), it later oscillates from prolate to oblate and back again, and finally settles on a sphere (with a ratio of 1).

In the 3D case, the gauge conditions and excision

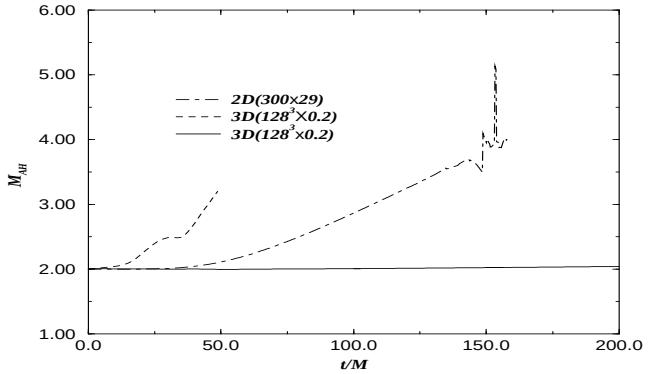

FIG. 3. The solid line shows the development of the AH mass M_{AH}, determined through a 3D AH finder, for the simulation of a Schwarzschild BH shown above, while the dashed lines show the AH mass obtained using 2D and 3D codes with no shift and no excision. The 2D code crashes at $t \simeq 150M$, the 3D run without shift crashes at $t \simeq 50M$, while the 3D run with shift and excision reaches an effectively static state and the error remains less than a few percent even after $t = 200M$.

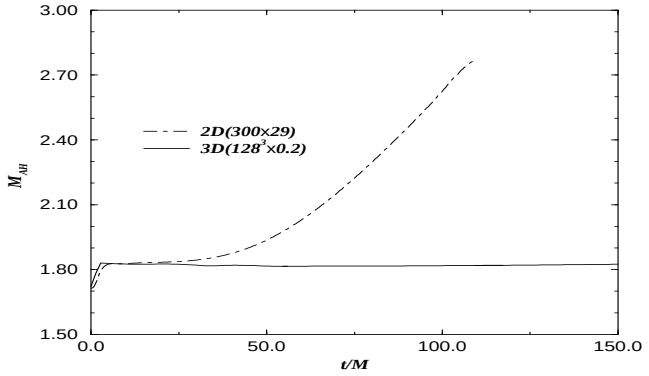

FIG. 4. We show the AH masses M_{AH} for a BH with even-parity distortion for the 2D (no excision, no shift) and 3D (excision, shift) cases. The 3D result continues well past $150M$, while the 2D result becomes very inaccurate and crashes by $t = 100M$.

quickly drive the metric to an almost static configuration, as the system itself settles towards a static Schwarzschild BH. The evolution is terminated at around $t = 160M$. To our knowledge, distorted BHs of this type have never been evolved for so long, nor with such accuracy, in either 2D or 3D. By comparison, in the more highly resolved 2D case with zero shift and no excision, the familiar grid stretching effects allowed by the gauge choice lead to highly inaccurate evolutions after some time with the error in M_{AH} again approaching 100% when the code finally crashes at $t \approx 100M$.

In Fig. 6, we show the results of extracting waves from the evolution of this highly distorted, excised BH. Using the standard gauge-invariant waveform extraction technique, the Zerilli function is shown for both the 2D and 3D simulations discussed above. There is a slight but physically irrelevant phase difference in the two results due to differences in the slicing; otherwise the results are

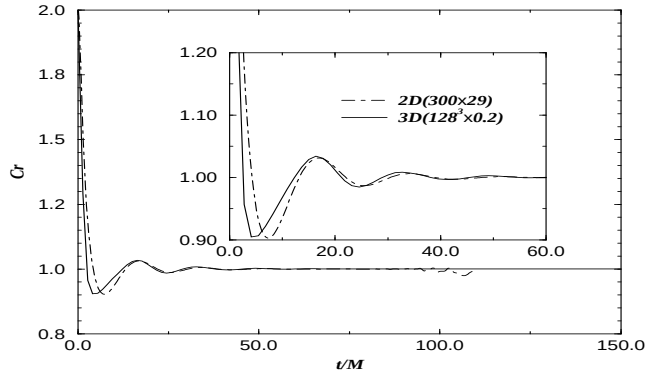

FIG. 5. We show the ratio of the polar and equatorial circumferences as a measure of the dynamics of the AH for the BH with even-parity distortion .

remarkably similar (the waves are extracted at the same Schwarzschild radius in both cases). This shows conclusively that the excision and live gauge conditions do not adversely affect the waveforms, even if they carry a small amount of energy (around $10^{-3}M_{ADM}$ in this case).

We now turn to a rather different type of distorted BH, including rotation and general even and odd-parity distortions. In the language of Ref. [17], the parameters for this simulation are $Q_0 = 0.5$, $\eta_0 = 0$, $\sigma = 1$, $J = 35$, corresponding to a rotating distorted BH with $M = 7.54$ and an effective rotation parameter $a/M = 0.62$. Previously, such data sets could be evolved only to about $40M$ [16]. For the purposes of this paper we have chosen an axisymmetric case so that we can compare the results to those obtained with a 2D code. Since this example is much more demanding, we have found it important in order to increase the accuracy of our runs to perform a single initial maximal solve to reduce the initial gauge dynamics. The symmetries of this example are now not consistent with the evolution of just one octant. However, we still have reflection symmetry on the $z = 0$ plane, so we evolve only the positive z half of the domain. The grid used in this case has $199^2 \times 100$ points and $\Delta x = 0.4$. The gauge conditions work well even in the presence of rotation: the shift drives the evolution to an almost static state as the system itself settles down to a *Kerr* BH. The metric functions (not shown) evolve in a similar way to those shown before, essentially freezing at late times. In Fig. 7, we show the extracted waveforms, now computed using the imaginary part of the Newman-Penrose quantity Ψ_4 (e.g. [3]), which includes contributions from all $\ell-$modes at the same time. The results from the 2D and 3D codes agree very closely, except for a slight phase shift due to slicing differences, until the 2D code becomes inaccurate and crashes. The 3D simulation continues well beyond this point, and is terminated at $t = 120M$.

Conclusions. We have extended recently developed 3D BH excision techniques, using a new class of live gauge conditions that *dynamically drive* the coordinates to a frame where the metric looks essentially static at late times, when the system itself settles to a stationary Kerr

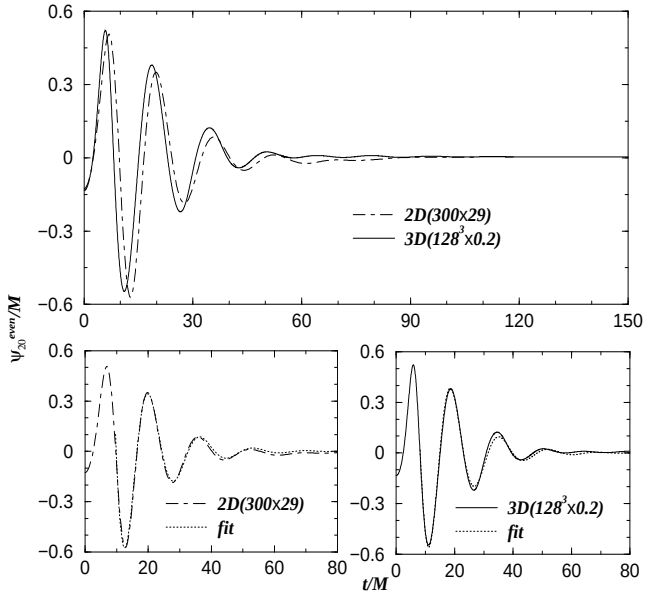

FIG. 6. The solid line shows the $\ell = 2, m = 0$ waveform extracted at a radius of $5.45M$ for the even-parity distorted BH described in the text, while the dashed line shows the result of the same simulation carried out in the 2D code. We also show a fit to the two lowest QNM's of the BH for 2D and 3D separately, using numerical data from $t = 9M$ to $t = 80M$.

BH. Our techniques have been tested on highly distorted, rotating BHs, and are shown to be very robust. For the first time, excision is tested with wave extraction, and waveforms are presented and verified. The results are shown to be more accurate, and much longer lived, than previous 3D simulations and even better resolved 2D simulations of the same data. Such improvements in BH excision are badly needed for more astrophysically realistic BH collision simulations, which are in progress and will be reported elsewhere.

Acknowledgements. This work was supported by AEI. Calculations were performed using the Cactus code at AEI, NCSA, PSC, and RZG.

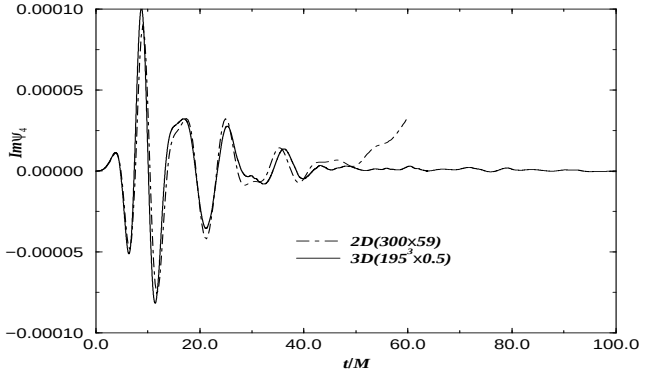

FIG. 7. The solid line shows the imaginary part of ψ_4 computed at $r = 3.94M$ and $\theta = \phi = \pi/4$ for a rotating distorted BH obtained from our $3D$ code with excision, while the dash line shows the same quantity computed using a $2D$ code (this simulation crashes at $t \simeq 60M$).

[1] L. Smarr and J. York, Phys. Rev. D **17**, 2529 (1978).
[2] M. Alcubierre *et al.*, (2000), gr-qc/0012079.
[3] J. Baker *et al.*, (2001), gr-qc/0102037.
[4] R. Gomez *et al.*, Phys. Rev. Lett. **80**, 3915 (1998).
[5] J. Thornburg, Class. Quan. Grav. **4**, 1119 (1987).
[6] E. Seidel and W.-M. Suen, Phys. Rev. Lett. **69**, 1845 (1992).
[7] G. B. Cook *et al.*, Phys. Rev. Lett **80**, 2512 (1998).
[8] M. Alcubierre and B. Brügmann, Phys. Rev. D **63**, 104006 (2001).
[9] S. Brandt *et al.*, Phys. Rev. Lett. **85**, 5496 (2000).
[10] L. E. Kidder, M. A. Scheel, and S. A. Teukolsky, (2001), gr-qc/0105031.
[11] P. Anninos *et al.*, Phys. Rev. D **52**, 2059 (1995).
[12] G. E. Daues, Ph.D. thesis, Washington University, St. Louis, Missouri, 1996.
[13] S. Brandt and E. Seidel, Phys. Rev. D **54**, 1403 (1996).
[14] S. Brandt and E. Seidel, Phys. Rev. D **52**, 870 (1995).
[15] K. Camarda and E. Seidel, Phys. Rev. D **59**, 064026 (1999), gr-qc/9805099.
[16] J. Baker *et al.*, Phys. Rev. D **62**, 127701 (2000), gr-qc/9911017.
[17] S. Brandt, K. Camarda, and E. Seidel, in *Proceedings of the 8th Marcel Grossmann Meeting on General Relativity*, edited by T. Piran (World Scientific, Singapore, 1999), pp. 741–743.
[18] S. Brandt, K. Camarda, and E. Seidel, in preparation (unpublished).
[19] R. A. Matzner, M. F. Huq, and D. Shoemaker, Phys. Rev. D **59**, 024015 (1999).
[20] M. Shibata and T. Nakamura, Phys. Rev. D **52**, 5428 (1995).
[21] T. W. Baumgarte and S. L. Shapiro, Physical Review D **59**, 024007 (1999).
[22] M. Alcubierre *et al.*, Phys. Rev. D **61**, 041501 (2000).
[23] M. Alcubierre *et al.*, Phys. Rev. D **62**, 124011 (2000).
[24] M. Alcubierre *et al.*, Phys. Rev. D **62**, 044034 (2000).
[25] C. Bona, J. Massó, E. Seidel, and J. Stela, Phys. Rev. Lett. **75**, 600 (1995).
[26] J. Balakrishna *et al.*, Class. Quant. Grav. **13**, L135 (1996).
[27] B. Brügmann, Int. J. Mod. Phys. D **8**, 85 (1999).
[28] M. Alcubierre *et al.*, Class. Quant. Grav. **17**, 2159 (2000).